Journal of Power Sources 185 (2008) 381–391

Contents lists available at ScienceDirect

Journal of Power Sources

journal homepage: www.elsevier.com/locate/jpowsour

Effect of inlet flow maldistribution in the stacking direction on the performance of a solid oxide fuel cell stack

Ping Yuan*

Department of Mechanical Engineering, Lee Ming Institute of Technology, 2-2, Lee Zhuan Road, Taishan, Taipei 243, Taiwan

ARTICLE INFO

Article history:
Received 1 May 2008
Received in revised form 11 June 2008
Accepted 11 June 2008
Available online 21 June 2008

Keywords:
Maldistribution
Performance
Solid oxide fuel cell
Stack
Numerical

ABSTRACT

This study examines the performance of a ten-cell solid oxide fuel cell (SOFC) stack with a non-uniform flow rate in the stacking direction. The author develops a two-dimensional numerical method to solve the electrochemical, mass and energy equations one stack at a time. The energy equations couple the heat exchange between the interconnector and both the cell and the flowing gas of adjacent cells. Moreover, this paper considers two boundary conditions, adiabatic and constant temperature, on the top and bottom faces of the SOFC. The results show that the non-uniform inlet flow rate of the fuel dominates the current density distribution; it causes the cell voltage to vary by over 13% for both boundary conditions. In addition, the constant temperature condition in this study can produce 3% more power than with the adiabatic condition. On the other hand, the air dominates the temperature field of a SOFC, and the non-uniform inlet flow rate of the air produces a variation of 3% in the average cell temperature of the cells when the boundary condition is adiabatic. This non-uniform effect on the electrical performance of each stack is apparently larger than in the transverse direction, which has been examined in our previous research.

1. Introduction

A solid oxide fuel cell (SOFC) includes two anode and cathode electrodes, and one solid electrolyte, between the anode and cathode, delivering oxygen ions from the cathode to the anode. Solid oxide fuel cells operate at high temperatures of about 600–1000 °C, and use methane or ethanol as fuel. Several recent studies have simulated their performance under different conditions, since the fuel rate, inlet temperature, operation pressure, cell size, etc. affect the temperature and current density distribution. Ferguson et al. [1] presented a three-dimensional mathematical model to examine the local distribution of electrical potential, temperature and concentration of chemical species in the SOFC. Yakabe et al. [2] modeled an anode-supported planar SOFC unit with counter-flow pattern double channels using a commercial package. The results indicated that the water-shift reaction, rather than the reforming reaction, effectively reduced the polarization concentration. Later, Yakabe et al. [3] simulated a planar SOFC three-dimensional model for a double channel unit using the same package. In that study, internal or external reforming steam, water-shift reaction, and gas diffusion considerations influenced its co-flow or counter-flow pattern model. Yuan et al. [4,5] numerically examined buoyancy and mass suction effects on the heat transfer and gas flow in a SOFC duct. Huang et al. [6] developed a multi-physics model coupling electrochemical kinetics with fluid dynamics to simulate transport phenomena in a mono-block-layer SOFC. This model improves the prediction of the local current density distribution, because it calculates locally the spatial variation of the cathodic and anodic surface over-potential. Janardhanan et al. [7] presented a performance analysis of a planar solid oxide fuel cell under direct internal reforming conditions. They used a model to study the influences of various operating parameters on cell performance, such as the air flow rate, anode thickness, steam to carbon ratio, specific area and pre-reforming. Their results pointed out that the efficiency of the fuel cell is higher for pre-formed fuel compared with non-reformed fuel. Araki et al. [8] examined a power generation system consisting of two SOFCs at different operating temperatures and in the serial connection. Their results showed that the power generation efficiency of the two-stage SOFC is somewhat higher than using only a high-temperature SOFC. Bedogni et al. [9] presented an experimental analysis of circular, planar, intermediate-temperature solid oxide fuel cells, and interpreted the experimental results using a finite volume model, which calibrated and validated the experimental voltage–current data. The comparison between the model and experiment demonstrated the capacity of the model to predict the cell behavior and overall energy

* Tel.: +886 2 29097811x1521; fax: +886 2 29095888.
E-mail address: pyuan@mail.lit.edu.tw.

0378-7753/$ – see front matter © 2008 Published by Elsevier B.V.
doi:10.1016/j.jpowsour.2008.06.039

Nomenclature

a	heat transfer area per based area ($m^2\ m^{-2}$)
c_p	specific heat capacity ($J\ mol^{-1}\ K^{-1}$)
d_{stack}	deviation of inlet molar flow rate in the stacking direction
E	Nernst voltage (V)
E_0	reversible open circuit voltage (V)
F	Faraday's constant (96,485 $As\ mol^{-1}$)
h	heat transfer coefficient ($W\ m^{-2}\ K^{-1}$)
i	current density ($A\ m^{-2}$)
i_0	exchange current density ($A\ m^{-2}$)
k	conductivity ($J\ m^{-1}\ K^{-1}$)
L	length in the x or y direction marked by a subscript x or y (m)
n	molar flow rate of fuel or air marked by a subscript f or a ($mol\ s^{-1}$)
$\bar{n}$	mean molar flow rate of fuel or air in the stack ($mol\ s^{-1}$)
n_{stack}	number of cells in stack
P	pressure
$\dot{q}_{reac}$	heat generation rate due to oxidation reaction ($W\ m^{-3}$)
r	area specific resistance of electrolyte ($\Omega\ m^{-2}$)
R	universal gas constant (=8.314 $J\ mol^{-1}\ K^{-1}$)
T	temperature (K)
V	cell voltage (V)
V_{act}	activation over-potential
V_{con}	concentration over-potential
V_{ohm}	ohmic over-potential
X	mole fraction of j-component indicated with a subscript j

Greek symbols

δ	thickness (m)

Subscripts

a	air
c	cell
c–a	interface between cell and air
c–f	interface between cell and fuel
f	fuel
i	interconnector
i–a	interface between interconnector and air
i–c	interface between interconnector and cell
i–f	interface between interconnector and fuel
j	components in fuel or air
x	x direction
y	y direction

balance even when significantly changing the cell operating conditions.

Achenbach [10] presented a three-dimensional simulation for the gas, current density and temperature distribution of a planar solid oxide fuel cell, which accounted for time-dependent effects, flow configurations, internal methane–steam reforming and recycling of the fuel. Recknagle et al. [11] simulated a three-dimensional SOFC unit with three kinds of flow pattern using the same commercial package used by [3] for reaction area performance. The authors showed temperature, current density, and fuel composition distributions with three flow configurations, co-flow, counter-flow, and cross-flow. Their results suggested that the co-flow configuration had the most uniform temperature distribution and smallest thermal gradients. Beale et al. [12] researched three different numerical methods for solving a single and ten-cell SOFC with cross-flow. The results showed that the direct numerical method is the most accurate method for a single cell. Simpler approaches can potentially supplant or complement the direct numerical method in fuel cell stack analysis. Iwata et al. [13] established a numerical program to estimate the temperature and current density profiles of a planar-type SOFC unit with co-flow, counter-flow and cross-flow. Their study examined the effects of the gas re-circulation ratio, operating pressure and physical properties on the current and temperature distributions. Recently, Wang et al. [14] built a fully three-dimensional mathematical model for a planar porous-electrode-supported SOFC to simulate steady-state electrochemical characteristics and multi-species/heat transport. Their results pointed out that the fuel and air are progressively heated along the flow direction, and the mass transport resistance of species in the porous anode under conditions of higher fuel utilization dominates the lowering of cell performance.

The flow configuration of a SOFC is similar to a heat exchanger, regardless of whether the flow configuration is co-flow, counter-flow or cross-flow. Because the fuel and air need manifolds to lead them into each stack, and distributors to assign the gases to channels in each stack, the manifold position and distributor geometry influence the flow rate distribution in the inlet section. The flow rate pattern in both the frontal entrance area and stacking direction are therefore non-uniform in practice. Costamagna et al. [15] researched non-uniform mass flow distribution in the stacking direction of a fuel cell with 100 cells. Boersma and Sammes [16] considered a non-uniform gas flow in the stacking direction along a solid oxide fuel cell stack, and employed a hydraulic resistance network to gain insight into its distribution. Recently, Okada et al. [17] proposed that a large-scale stack be divided into four blocks from the viewpoint of the gas flow scheme, with gas supplied uniformly to each stack. This method could improve the prospects for 200 kW cells.

Few reports have examined the effects of non-uniform inlet flow on fuel cell temperature and current density. Hirata and Hori [18] used a numerical method to examine the relationships between planar and stacking direction gas flow uniformities, and cell performance in a co-flow type fuel cell. Liu et al. [19] as well as Yuan and Liu [20] developed a reliable numerical method to examine the effect of inlet flow maldistribution in the transverse direction on the thermal and electrical performance of a MCFC and SOFC unit

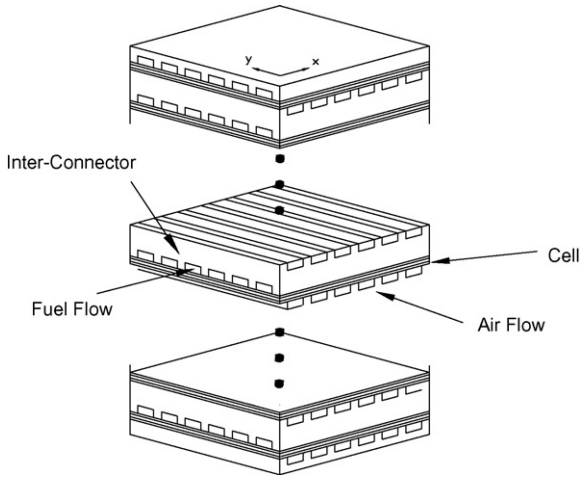

Fig. 1. Schematic diagram of a unit in a solid oxide fuel cell stack with cross-flow configuration.

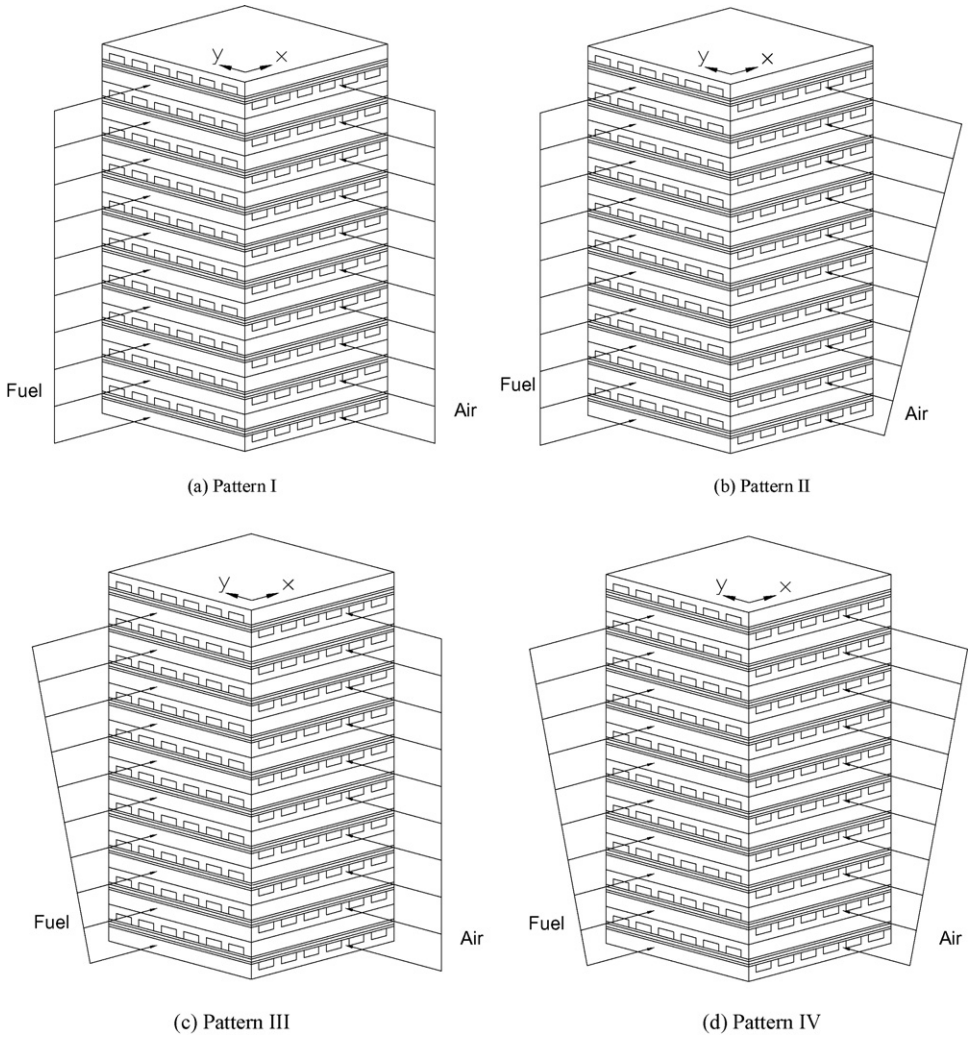

Fig. 2. Various inlet flow patterns in an SOFC stack.

with cross-flow configuration. Their results showed that the non-uniform inlet flow affects only slightly the average temperature and average current density, but induces greater non-uniformities of temperature and current density for most maldistribution patterns. For a SOFC stack, the non-uniform gas flow rate in each stack is severe because of the gas manifold [15–17]. Although the non-uniform inlet flow in the transverse direction affects only the temperature and current density distribution and not the average temperature and current density, the different flow rates in each stack caused by the maldistribution in the stacking direction must induce different average temperatures and current densities. Previous literature [1–14] has examined the performance of a SOFC stack, but none has focused on the effect of non-uniform inlet flow in the stacking direction on the SOFC stack performance. Some research [15–17] identified an obvious maldistribution of the gas flow rate in the stacking direction of a fuel cell stack. Therefore, looking into the non-uniform effect of gas flow rate on the thermal and electrical performance of a SOFC stack is worthwhile and practical.

2. Description of the theory

This study plans to analyze the thermal and electrical performance of a solid oxide fuel cell stack, formed by connecting 10 unit cells as shown in Fig. 1. In this figure, the unit cell from top to bottom includes the interconnector with the flow channels, fuel, anode, electrolyte, cathode and air. To simplify the analysis, this study combines the anode, cathode, and electrolyte into one unit termed the cell. The unit cell is 0.2 m × 0.2 m in the x–y plane, and the fuel and the air flows along the interconnecting channels as well as along the x and y direction. Fig. 2 shows the whole SOFC stack with various inlet flow distributions. This study considers a uniform profile and a progressively increasing profile in the stacking direction to construct four patterns of non-uniform inlet flow. Before formulating the governing equations for the SOFC stack, this study assumes some idealizations to simplify the analysis, as follows:

(1) The inlet temperature and mole fractions of species in the fuel and the air are constant and uniform over all cells.
(2) The thermal properties of fuel, air, cell and interconnector are constant, except for the specific heat capacities of the fuel and the air.
(3) The boundaries of the SOFC stack in the x–z and y–z plane are adiabatic; the boundary on the top and bottom faces of the SOFC stack is either adiabatic or at constant temperature.
(4) The change in the z direction of each cell is negligible.
(5) The cross-sectional geometry of the inter-connections is unchanged throughout the x–y plane.

Table 1
Parameters and conditions in this study

Mole flow rate and molar fraction of species in anode inlet	
N_f	0.09 mol s^{-1}
X_{H_2}	0.36
X_{CO_2}	0.05
X_{H_2O}	0.05
X_{CO}	0.35
X_{N_2}	0.19
Mole flow rate and molar fraction of species in cathode inlet	
N_a	0.18 mol s^{-1}
X_{O_2}	0.22
X_{N_2}	0.78
Inlet temperature (K)	
T_f	898
T_a	898
Operation pressure (Pa)	
P	1×10^5
Conductivity (W m^{-1} K^{-1})	
k_c	2
k_i	13
k_{i-c}	1
Heat transfer area per unit base area (m^2 m^{-2})	
$a_{i-f} = a_{i-a}$	1.0
$a_{c-f} = a_{c-a}$	0.5
a_{i-c}	1.0
Thickness (m)	
δ_c	0.6×10^{-3}
δ_i	3×10^{-3}
δ_{i-c}	1.8×10^{-3}
Deviation in the stacking direction	
d_{stack}	0.5

(6) The cell voltage is uniform over the cell plane.
(7) The water-shift reaction in the fuel is negligible.

2.1. Governing equations

2.1.1. Reaction equations

This study considers the use of reformed methane or ethanol in the external reformer. The reformed gases are fed into the SOFC, so that the feed fuel includes hydrogen (H_2), nitrogen (N_2), carbon dioxide (CO_2), carbon monoxide (CO) and water (H_2O). The anode oxidation reactions are as follows:

$$CO + O^{2-} \rightarrow CO_2 + 2e^- \quad (1)$$

$$H_2 + O^{2-} \rightarrow H_2O + 2e^- \quad (2)$$

The reaction at the cathode is

$$O_2 + 4e^- \rightarrow 2O^{2-} \quad (3)$$

2.1.2. Mass balance equations

Flow through the fuel and air channels can be assumed to be one-dimensional and laminar (plug flow) so this study takes the conservation of mass for each species. The left term represents the molar flow rate change in the fuel and the air, and the right term represents the species consumption linking the local current density:

$$\left(\frac{1}{L_y}\frac{d(n_f X_j)}{dx}\right)^k = \left(\pm\frac{i}{2F}\right)^k \quad (4)$$

$$\left(\frac{1}{L_x}\frac{d(n_a X_j)}{dy}\right)^k = \left(-\frac{i}{4F}\right)^k \quad (5)$$

Meanwhile, the plus or minus symbol represents the dependence of the molar flow rate (increase or decrease) on the reactant or product species. In Eq. (4), fuel reactants and products include hydrogen, carbon monoxide, carbon dioxide and water. The reactant and product in air includes only oxygen, as in Eq. (5). The superscript k stands for the stack number.

2.1.3. Energy balance equations

This study takes into consideration the conservation of energy for the fuel, air, cell, and interconnector for each stack. It is noted that the energy conservation expression for the interconnector contains the heat exchange terms between itself and the air as well as between itself and the cell in the next stack. Therefore, the interconnector temperature interacts with the gas and cell temperature in the next stack, as well as the energy equations that couple the temperature interaction in the whole stack. The energy conservation equations for the fuel, air, cell, and interconnector are as follows, respectively:

$$\frac{d}{dx}\left(\sum n_f X_j c_{p,j} T_f\right)^k = (ha)_{i-f}(T_i^k - T_f^k) + (ha)_{c-f}(T_c^k - T_f^k) + \frac{i}{4F} c_{p,O_3{}^{2-}} T_c^k \quad (6)$$

$$\frac{d}{dy}\left(\sum n_a X_j c_{p,j} T_a\right)^k = (ha)_{i-a}(T_i^{k-1} - T_a^k) + (ha)_{c-a}(T_c^k - T_a^k) - \frac{i}{4F} c_{p,O_3{}^{2-}} T_a^k \quad (7)$$

$$\begin{aligned} &-(k\delta)_c \frac{\partial^2 T_c^k}{\partial x^2} - (k\delta)_c \frac{\partial^2 T_c^k}{\partial y^2} \\ &= (ka)_{i-c}\frac{(T_i^k - T_c^k)}{\delta_{i-c}} + (ka)_{i-c}\frac{(T_i^{k-1} - T_c^k)}{\delta_{i-c}} \\ &\quad + (ha)_{c-f}(T_f^k - T_c^k) + (ha)_{c-a}(T_a^k - T_c^k) + \frac{i}{4F} c_{p,O_3{}^{2-}} T_a^k \\ &\quad - \frac{i}{4F} c_{p,O_3{}^{2-}} T_c^k + \dot{q}_{reac}^k \end{aligned} \quad (8)$$

$$\begin{aligned} &-(k\delta)_i \frac{\partial^2 T_i^k}{\partial x^2} - (k\delta)_i \frac{\partial^2 T_i^k}{\partial y^2} \\ &= (ka)_{i-c}\frac{(T_c^k - T_i^k)}{\delta_{i-c}} + (ka)_{i-c}\frac{(T_c^{k+1} - T_i^k)}{\delta_{i-c}} \\ &\quad + (ha)_{i-f}(T_f^k - T_i^k) + (ha)_{i-a}(T_a^{k+1} - T_i^k) \end{aligned} \quad (9)$$

The specific heat capacities of each gas species in the fuel and the air are a function of temperature [21]. This study selects half of the oxygen specific heat capacity as the oxygen ion specific heat capacity. In Eqs. (6)–(8), the term $ic_{p,O^{2-}}T/4F$ describes the heat transfer rate as the oxygen ion migrates from the air side to the fuel side through the cell. In Eq. (8), $\dot{q}_{rect}$ is the heat generated in the cell unit because of electrochemical reactions and cell internal losses [22], generated over the x–y plane as follows:

$$\dot{q}_{rect} = -\Delta H \frac{i}{2F} - Vi \quad (10)$$

$$\Delta H = -240,506 - 7.3835 T_c \quad (11)$$

Meanwhile, ΔH is the enthalpy change per mole of the chemical reaction, calculated as a function of temperature [21]. In Eqs. (8) and (9), k_{i-c} is the thermal conductivity due to contact resistance between the cell and interconnector in the z direction, and its value is set to 1.0 W m^{-1} K^{-1}.

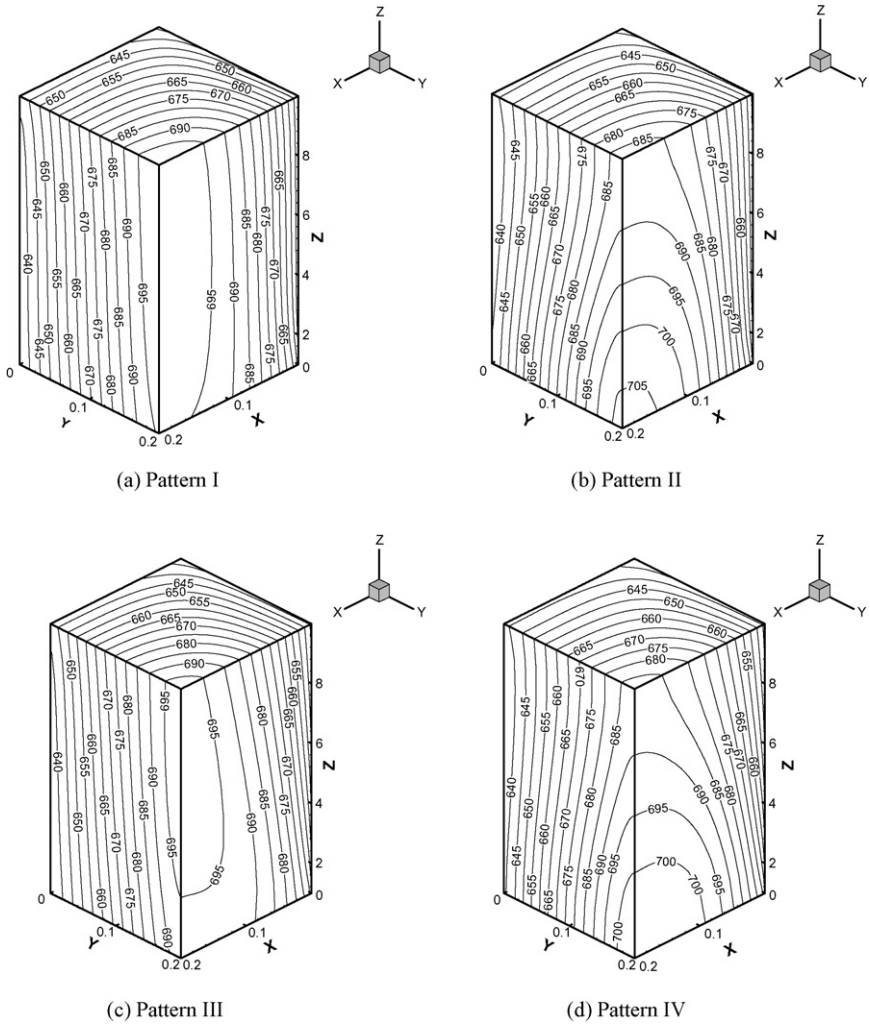

Fig. 3. Cell temperature distribution on the exit faces and top face of an SOFC stack in the adiabatic condition.

The molar flow rate of the fuel and the air in each stack, n_{f}^{k} and n_{a}^{k}, is different because of the non-uniform distribution of molar flow rates in the stacking direction. In this study, the non-uniform flow pattern in the stacking direction has a progressively increasing profile, so the molar flow rate of each stack can be expressed in terms of the stack number as follows:

$$n_{\mathrm{f}}^{k} = \bar{n}_{\mathrm{f}} \left(\frac{2d_{\mathrm{stack,f}}^{k}}{(n_{\mathrm{stack}} - 1)}(k-1) + (1 - d_{\mathrm{stack,f}}^{k}) \right) \tag{12}$$

$$n_{\mathrm{a}}^{k} = \bar{n}_{\mathrm{a}} \left(\frac{2d_{\mathrm{stack,a}}^{k}}{(n_{\mathrm{stack}} - 1)}(k-1) + (1 - d_{\mathrm{stack,a}}^{k}) \right) \tag{13}$$

In the above equations, $\bar{n}_{\mathrm{f}}$ and $\bar{n}_{\mathrm{a}}$ represents the mean flow rate of the fuel and the air in the SOFC stack, and the molar flow rate in each stack depends on the deviation in the stacking direction, d_{stack}, as well as the total number of cells, n_{stack}. The deviation in the stacking direction is the ratio of the variation of flow rate to the mean flow rate; its value may be positive or zero, representing the progressively increasing profile and uniform profile, respectively.

2.1.4. Nernst voltage and over-potentials

The Nernst voltage is an ideal potential, and it is calculated by the following equation:

$$E^{k} = E_{0}^{k} + \frac{RT^{k}}{2F} \ln \left(\frac{P_{\mathrm{H_2}}^{k} P_{\mathrm{O_2}}^{k0.5}}{P_{\mathrm{H_2O}}^{k}} \right) \tag{14}$$

$$E_{0}^{k} = 1.2723 - 2.7654 \times 10^{-4} T_{\mathrm{c}}^{k} \tag{15}$$

Meanwhile, E_0 is the ideal voltage for hydrogen oxidation at standard pressure. This study considers the voltage loss caused by electrolyte ohmic polarization, electrode activation polarization and concentration polarization. Because concentration polarization in the cathode is less than in the anode when the SOFC cell is electrolyte-supported and anode-supported, this study neglects concentration polarization in the cathode [23]. Therefore, the cell voltage equals the Nernst voltage minus the polarization voltages (ohmic, activation and concentration) in the anode, as follows:

$$V^{k} = E^{k} - V_{\mathrm{ohm}}^{k} - V_{\mathrm{act}}^{k} - V_{\mathrm{con}}^{k} \tag{16}$$

$$V_{\mathrm{ohm}}^{k} = i^{k} r \tag{17}$$

$$V_{\mathrm{act}}^{k} = \frac{RT_{\mathrm{c}}^{k}}{2F} \sinh^{-1} \left(\frac{i^{k}}{2i_{0,\mathrm{anode}}} \right) + \frac{RT_{\mathrm{c}}^{k}}{2F} \sinh^{-1} \left(\frac{i^{k}}{2i_{0,\mathrm{cathode}}} \right) \tag{18}$$

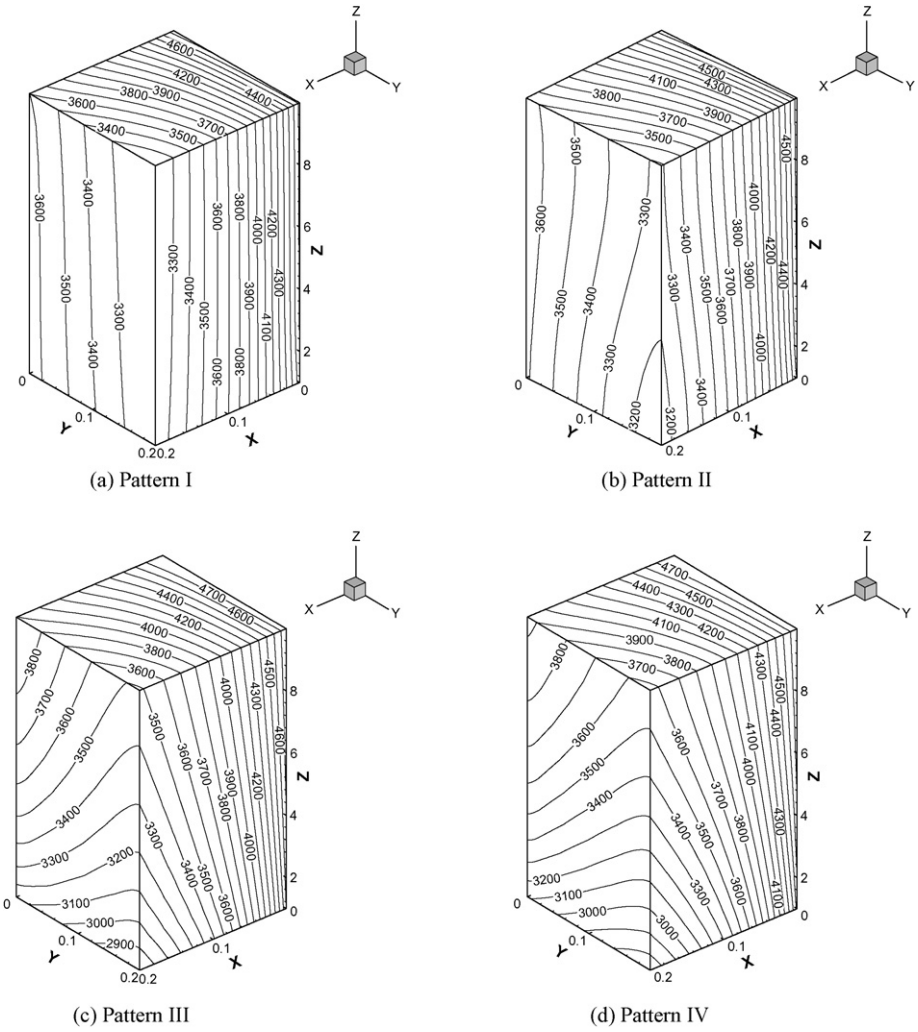

Fig. 4. Current density distribution on the exit faces and top face of an SOFC stack in the adiabatic condition.

$$V_{\mathrm{con}}^{k} = -\frac{RT_{\mathrm{c}}^{k}}{2F}\ln\left[\frac{1-(RT_{\mathrm{c}}^{k}/2F)(\delta_{\mathrm{anode}}/D_{\mathrm{anode}}p_{\mathrm{H_2}})i^{k}}{1+(RT_{\mathrm{c}}^{k}/2F)(\delta_{\mathrm{anode}}/D_{\mathrm{anode}}p_{\mathrm{H_2O}})i^{k}}\right] \tag{19}$$

Here r is $300\times10^{-7}\,\Omega\,\mathrm{m}^{-2}$ [24], $i_{0,\mathrm{anode}}$ and $i_{0,\mathrm{cathode}}$ are 1290 and $970\,\mathrm{A\,m^{-2}}$ [25], respectively, δ_{anode} is 0.05 mm, and D_{anode} is $2\times10^{-5}\,\mathrm{m\,s^{-1}}$ [26]. The method of solving these governing equations in a SOFC unit has been developed in the author's previous research [20]. The method uses mass and energy balance equations to solve the mole fraction of each species, as well as the temperatures of the fuel, air, cell, and interconnector. The solving method then calculates the current density from Eqs. (16) to (19), based on the assumption that the cell voltage is uniform over the cell reaction area.

3. Numerical methods

This study uses a finite difference method to solve the governing equations in each stack one by one. In each stack calculation, there are four two-dimensional domains, each with area $0.2\,\mathrm{m}\times0.2\,\mathrm{m}$. Every calculation domain is divided into $N\times N$ subdivisions, and both the inlet and exit of the fuel and the air subdivisions are assigned the calculation nodes of the gas molar flow rate and the temperature. Moreover, this study assigned the calculation nodes of cell temperature and current density to be in the center of the cell subdivisions, and assigned the calculation nodes of the interconnector temperature to be in the center of the interconnector subdivisions. The author discretizes Eqs. (4)–(9) to be finite difference equations by an implicit scheme and the node arrangement described above. This work then uses Fortran code to solve the gas molar flow rate of each species in the fuel and air, the temperatures of the fuel, air, cell and the interconnector, as well as the current density; these are the variables in the finite difference equations. The calculation proceeds as follows. (1) The program guesses a uniform current density distribution and solves the molar flow rate of each species in the fuel and air using Eqs. (4) and (5) in the first stack. (2) The program solves the temperature fields of the fuel, air, cell and interconnector using Eqs. (6)–(9), respectively, in the same stack. (3) Then the Nernst voltage is calculated from Eq. (14) and the Newton–Raphson iteration is used to solve the current density in the same stack through Eqs. (16)–(19) by setting a constant cell voltage. (4) The current density is updated and the loop from Step 1 to Step 3 is repeated until all relative errors of the molar flow rates, temperature and current density satisfy the convergence criteria. (5) The calculations in Step 1 to Step 4 are repeated for the next stack ($k+1$), and so on to the end stack and then calculating back to the first stack. (6) Step 5 is repeated and the program checks the relative errors of the interconnector temperature in all cells between the adjacent calculation loops in Step 5, and the whole calculation stops when the relative error satisfies the convergence criteria. The numerical method for calculating

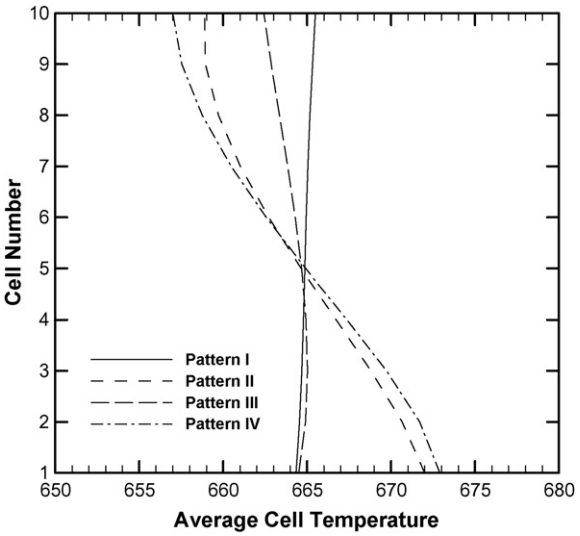

Fig. 5. Average cell temperature of each cell in the adiabatic condition.

a SOFC unit has been validated in previous research [20], so the procedure of adding an iteration scheme in this study for calculating the temperature and current density field in an SOFC stack is known to be reliable. Table 1 lists all the parameters and conditions in the FORTRAN program. In addition, the convection heat transfer coefficient is calculated from $Nu = 3.146$ when the flow is laminar and fully developed in a rectangular duct, and the effective contact thickness between cell and interconnector is the average thickness of the cell and interconnector.

4. Results and discussion

Fig. 3 depicts the cell temperature distributions at the exit and the top face of an SOFC stack with adiabatic boundary conditions on the top and bottom cells as well as for different inlet flow patterns, including uniform fuel and air in Pattern I, uniform fuel and non-uniform air in Pattern II, non-uniform fuel and uniform air in Pattern III, and finally non-uniform fuel and air in Pattern IV. Fig. 3(a) shows that the temperature increases along the flow directions of both the fuel and the air, and it approaches the highest temperature (over 695 °C) in the exit corner. Examining the temperature contours on the exit faces indicates that all are nearly vertical lines except those near the bottom stack. This means that the temperature distribution in each stack is similar, and the highest temperature in the bottom stack is a little lower than that in the other cells. Examining Fig. 2 indicates that the air flows through the bottom interconnector, and the fuel flows through the top interconnector. Because the flow rate of air is obviously greater than that of the fuel, the air has a stronger cooling ability than the fuel. Therefore, the cell temperature at the bottom stack is slightly lower than at the top stack when both the boundary conditions on the top and bottom are adiabatic. This effect on the cell temperature can be neglected because the temperature difference between the top and the bottom cells is below 5 °C. Fig. 3(b) shows the cell temperature contours on the exit and top faces of the SOFC stack for Pattern II, and indicates that the non-uniform inlet flow rate of the air strongly affects the outline of the temperature compared to Fig. 3(a). In a fuel cell, the molar flow rate of the air is always greater than the fuel, because the air not only provides the oxygen for chemical reaction but also plays the role of cooling. This study considers the non-uniform inlet flow rate of the air progressively increases along the stacking direction, because the position of the inlet manifold is located at the top. Consequently, the cooling effect of the air increases along the stacking direction, and so the cell temperature decreases along this direction. The temperature difference between the top and bottom stack in Fig. 3(b) is close to 20 °C, and the difference becomes larger with an increase in the deviation of the stacking direction. Fig. 3(c) shows the temperature contour on the exit and top faces of the SOFC stack in Pattern III, which has non-uniform inlet fuel flow and uniform inlet air flow. The temperature outline in this figure is similar to that in Fig. 3(a), which has both uniform inlet fuel and air flow. Because the air dominates the temperature distribution due to its larger molar flow rate compared to the fuel, the contour in Fig. 3(c) is close to that in Fig. 3(a). Although the non-uniform inlet fuel flow slightly affects the temperature contour in Fig. 3(c), the progressively increasing profile of the inlet molar flow rate induces somewhat lower temperatures (about 5 °C) on the bottom stack compared to those in Fig. 3(a). This temperature drop is a result of the reduction of the heat of reaction due to the lower molar flow rate of the fuel. Fig. 3(d) depicts the temperature distribution on the exit and top faces of the SOFC stack in Pattern IV, which has non-uniform inlet molar flow for both fuel and air. According to the arguments above, the air dominates the cell temperature distribution and the effect of non-uniform inlet molar flow rate of fuel is ignored, so it is clear that the contour in Fig. 3(d) is similar to that in Fig. 3(b) because of the same non-uniform air flow pattern. The slight difference between Fig. 3(b) and (d) is near the bottom stack, because the non-uniform inlet molar flow rate of the fuel induces less reaction heat due to the lower fuel flow in the bottom stack in Pattern IV.

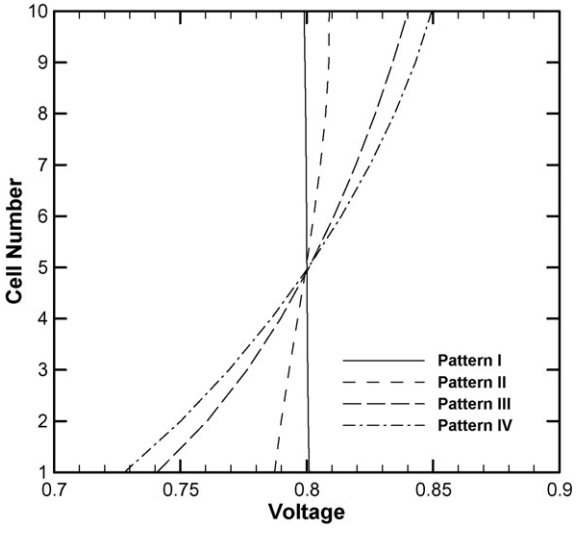

Fig. 6. Cell voltage of each cell in the adiabatic condition when the current density is 3900 A m^{-2}.

To calculate the electrical performance from Eqs. (16)–(19), this study considers that the cells are connected in parallel, and calculates the current density distribution in each stack when the cell voltage is assumed to be constant. Fig. 4 shows the current density contour on the faces of the exit and top in the SOFC stack when the deviation of inlet molar flow rate in the stacking direction is 0.5. In this figure, it is clear that the outline of these contours in Pattern I and Pattern II are similar, and so are those in Pattern III and Pattern IV. Pattern I and Pattern II have same inlet molar flow rate of fuel, but different inlet molar flow rates of air. Comparing Fig. 4(a) and (b) shows that the non-uniform inlet molar flow rate of the air slightly affects the current density distribution in a SOFC stack; it raises the current density on the top stack and reduces it on the

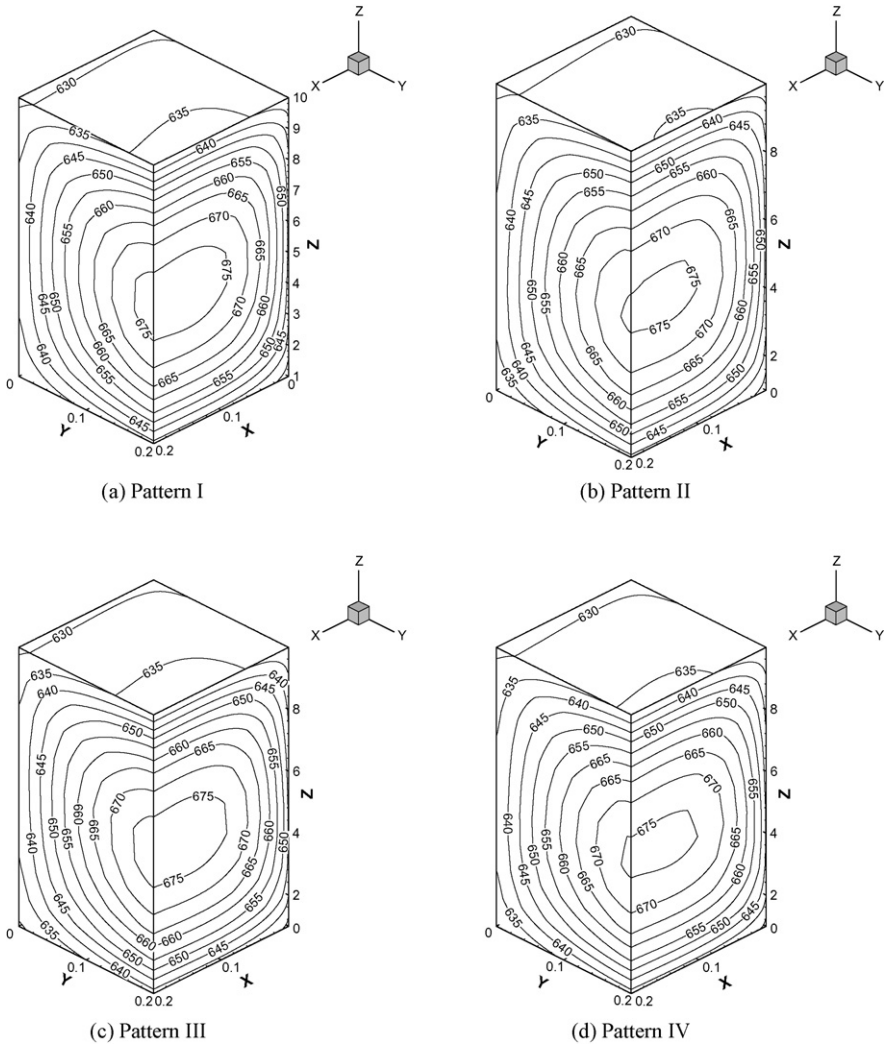

Fig. 7. Temperature distribution on the exit faces and top face of an SOFC stack in constant temperature condition.

bottom stack (Fig. 4(b)). Examining the difference of average current density in each stack between Pattern I and Pattern II indicates that all changes are below 0.5%. Therefore, the effect of the non-uniform inlet flow rate of the air in the stacking direction on the electrical performance of a SOFC stack is ignored. The current density contours of Pattern III and Pattern IV are similar (Fig. 4(c) and (d)). The change rates of the average current density in each stack based on in Pattern I are over 5%. Because Pattern III and Pattern IV have the same inlet condition with a non-uniform molar flow rate of fuel, the effect of the fuel non-uniform inlet flow in the stacking direction on the electrical performance of a SOFC stack is stronger than the effect of the non-uniform air inlet flow. Comparing Fig. 4(c) and (d) shows that the non-uniform inlet molar flow rate of the air slightly affects the current density distribution; it raises the current density on the top stack and reduces it on the bottom stack. Examination of the contours of the current density in Fig. 4(c) and (d) shows that the current density increases along the stacking direction. The average current density increases from 3574 A m^{-2} on the bottom stack to 4171 A m^{-2}, on the top stack in Pattern IV, and has a change rate of 15%. It is noted that a greater flow rate for the fuel will maintain a higher concentration of hydrogen and produce a higher current density. The non-uniform inlet molar flow rate of the fuel in this study increases progressively from the bottom to the top, so the current density will increase along the stacking direction. In a fuel cell, the molar flow rate of fuel is always restricted in order to reduce the wastage of hydrogen, so the manifold design for producing uniform inlet flow in the stacking direction is very important for maintaining uniform electrical performance.

Fig. 5 depicts the average cell temperature for different cells in four patterns when the deviation of the non-uniform inlet flow rate in the stacking direction is 0.5. As mentioned in Fig. 3, the effect of the non-uniform inlet molar flow rate of the fuel can be neglected, so the average cell temperatures in Pattern I and Pattern III are nearly uniform among the cells in Fig. 5. Meanwhile, the average cell temperature on the top stack in Pattern III becomes lower than in Pattern I, because of the greater fuel flow rate on this stack due to the progressively increasing non-uniform profile of the fuel in the stacking direction. This greater fuel flow rate provides a greater cooling effect on the top stack compared to the line of Pattern I. In this figure, the average cell temperature profiles along the stacking direction in Pattern II and Pattern IV are obviously different to those in Pattern I and Pattern III, because the non-uniform inlet molar flow rate of the air dominates the temperature distribution of the SOFC stack. Since the molar flow rate of the air increases in the direction of stacking, the cooling effect of the air increases along this direction. Although the total average of cell temperatures in the whole SOFC stack is the same in different patterns, the difference of average cell temperature among different cells in Pattern I,

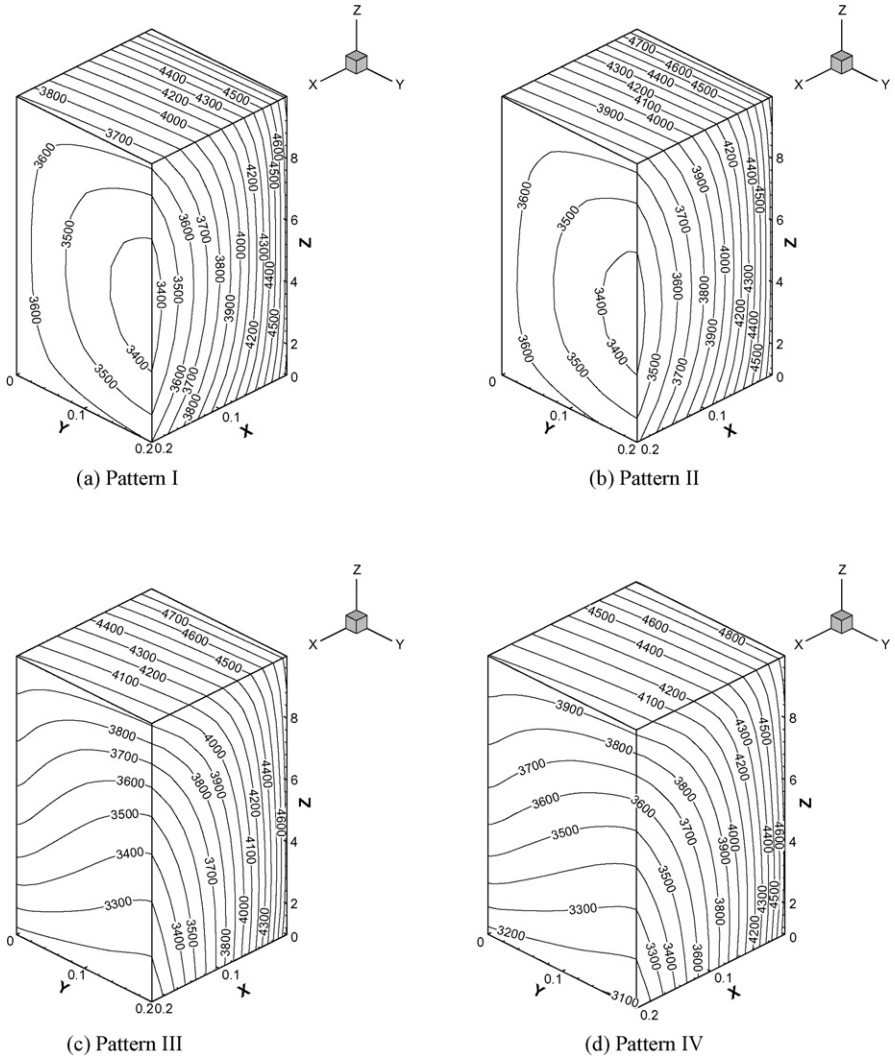

Fig. 8. Current density distribution on the exit faces and top face of an SOFC stack in constant temperature condition.

Pattern II, Pattern III, and Pattern IV are 1.2, 11.8, 2.8, and 15.9 °C, respectively. This result shows that the effect of the non-uniform inlet molar flow of the air in the stacking direction is important to the thermal performance in a SOFC stack.

When cells in the SOFC are connected in series, the calculated results based on constant cell voltage can be changed to results based on constant current, according to the conservation of power output. Fig. 6 shows the cell voltage in different cells when the flow pattern is I, II, III, and IV. In this figure, the cell voltage profile along the stacking direction in Pattern I is the most uniform, with a value of 0.8 V. The cell voltage profile in Pattern II is close to 0.8 V, because of the non-uniform inlet molar flow rate of the air. The non-uniform inlet molar flow rate of the fuel dominates the electrical performance, so the cell voltage profiles in Pattern III and Pattern IV are obviously different to those in Pattern I and Pattern II. In this figure, the average current density of each stack is set to be 3900 A m^{-2}, and the total voltage of this SOFC stack for all patterns is 8.1 V. Moreover, the variation rate of cell voltage among different cells is 0.3%, 2.7%, 12.4%, and 15.0% in Pattern I, Pattern II, Pattern III, and Pattern IV, respectively. Although the total electrical power seems to be slightly affected by the non-uniform inlet molar flow rate in the stacking direction, the very different cell voltages in these cells due to the non-uniform inlet molar flow rate will adversely affect the operation of the SOFC stack, inducing durability and material problems. Therefore, the uniform inlet fuel in the stacking direction is a key point in the design of a distributor in a SOFC stack.

Fig. 7 shows the cell temperature contour on the exit and top faces of a SOFC stack for different patterns when the top and bottom boundary conditions are set to a constant temperature of 625 °C, which is the inlet temperature of both the fuel and the air. In this figure, it is clear that the non-uniform inlet molar flow rate of both the fuel and air affect only slightly the cell temperature distribution of this SOFC stack. The cell temperatures in all patterns are between 635 and 675 °C, and the maximum temperature occurs at the exit corner of the fuel and the air in the central stack. The cell temperature range in Fig. 7 is smaller than that in Fig. 3, which has adiabatic boundary conditions on the top and bottom stack. Therefore, the constant temperature boundary condition is better than the adiabatic boundary condition, because the variation in cell temperature becomes small, and the position of the maximum temperature is fixed despite the non-uniform inlet molar flow rate of the fuel and the air. In practice, it is easier to arrive at the constant temperature boundary conditions on the top and bottom stack, when the air flows through the top and bottom of the SOFC stack before it flows into the fuel cell.

Fig. 8 shows the current density distribution on the exit and top faces of the SOFC stack for different patterns when the boundary

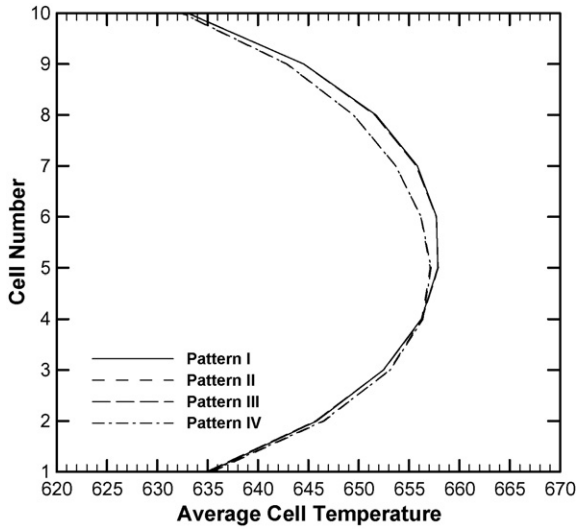

Fig. 9. Average cell temperature of each cell in the constant temperature condition.

condition for the top and bottom stack is a constant temperature of 625 °C. In Fig. 8(a) and (b), the contours of current density are familiar, because the non-uniform inlet molar flow rate of the air affects only slightly the current density distribution, as mentioned before. Due to the constant temperature boundary condition, the current density distributions are totally different to those in Fig. 4(a) and (b). Moreover, the minimum current density also occurs at the exit corner in the central stack, close to the hot spot location in Fig. 7, because the higher temperature induces a lower Nernst voltage. In Fig. 8(c) and (d), the current density distribution is obviously still affected by the non-uniform inlet molar flow rate of the fuel in the stacking direction, because the current density drop along the fuel flow direction of x in the bottom stack is greater than in the top stack. Comparing Figs. 4–8 shows that the current density at constant temperature is higher than under adiabatic conditions. Examining the calculation results of the current density shows the promotion of average current density of the SOFC stack is close to 3% because of the constant temperature condition. Therefore, the constant temperature boundary condition on the top and bottom stack is preferable to the adiabatic boundary condition based on consideration of the thermal and electrical performance.

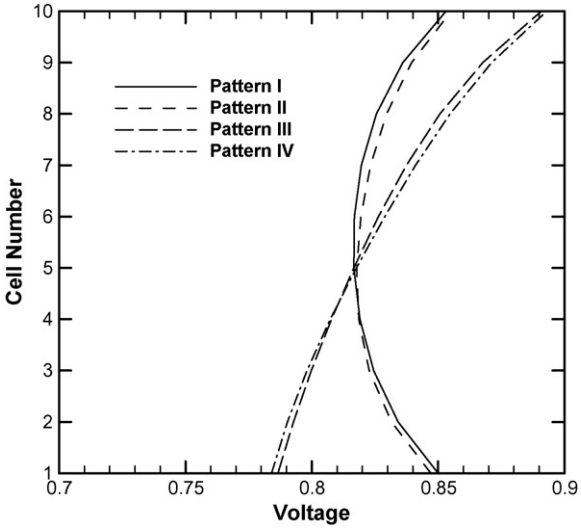

Fig. 10. Cell voltage of each cell in the constant temperature condition when the current density is 3900 A m^{-2}.

Fig. 9 shows the average cell temperature of different cells when the boundary condition on the top and bottom cells is a constant temperature of 625 °C. In this figure, the temperature range is from 635 to 658 °C, a range which is larger than in Fig. 5 for the adiabatic boundary condition. Although this temperature range becomes greater than in Fig. 5, the maximum temperature decreases because of the constant temperature boundary condition. This means that the constant temperature boundary condition benefits control of the maximum temperature in the core of the SOFC stack. Also, the effect of the non-uniform inlet molar flow rate of the fuel and the air on the average cell temperature is extremely small for the constant temperature boundary condition, and can be ignored. This means that the constant temperature boundary condition is better than the adiabatic boundary condition, and an engineer can easily achieve this situation using the waste heat in a SOFC power plant to maintain the constant temperature at the top and the bottom boundaries of a SOFC stack. Fig. 10 depicts the cell voltage in different cells when the cells are connected in series. As mentioned in Fig. 6, this study uses the numerical results with an assumption of constant voltage to recalculate the cell voltage with constant current density. In Fig. 10, the constant current density is set at 3900 A m^{-2}, so the cell voltage can be determined from the conservation of power. In this figure, it is clear that the cell voltage profiles in Pattern I and Pattern II are similar and more uniform than those in Pattern III and Pattern IV. The variation of cell voltage in Pattern I, Pattern II, Pattern III, and Pattern IV is 4%, 5%, 13%, and 13%, respectively. This shows that the non-uniform inlet molar flow rate of the fuel in the stacking direction induces larger cell voltage variations. Comparing the cell voltage in Fig. 10 to that in Fig. 6 shows that the cell voltage in Fig. 10 is higher than in Fig. 6. This means that the constant temperature boundary condition on the top and bottom stack is better than the adiabatic boundary condition. The constant boundary temperature will affect the electrical performance, and the cell voltage will decrease with an increase in the temperature on the boundary face, because the higher temperature induces a lower Nernst voltage. Therefore, it can promote the electrical performance of a SOFC stack by means of suitable temperature control on the top and the bottom faces of the SOFC stack.

5. Conclusions

This study examined the three dimensional temperature and current density distribution in a SOFC stack with four different inlet flow patterns in the stacking direction. The author used a two-dimensional numerical method to solve the mass conservation, energy conservation, and chemical reaction equations through each stack, one by one, and then obtained the whole temperature field and current density field by this iteration scheme. In addition, the average current densities in different cells can be transformed to the cell voltage based on the conservation of power when the SOFC cells are connected in series. The results show that the non-uniform inlet molar flow rate of the fuel dominates the current density distribution for both constant temperature and adiabatic boundary conditions. The effect of non-uniform inlet flow of the fuel on the variation of current density for connection in parallel or on the variation in cell voltage when connected in series are both close to 15% for Pattern III and Pattern IV when the boundary condition is adiabatic, and 13% in the Pattern III and Pattern IV when the boundary condition is a constant temperature. Moreover, the constant temperature boundary condition of 625 °C can promote 3% more power than the adiabatic boundary condition did. Therefore, the constant temperature boundary condition on the top and bottom cells of a

SOFC is to be preferred, and it is easy to maintain in a SOFC power plane using the waste gas. On the other hand, the air dominates the temperature field of a SOFC stack, and the non-uniform inlet molar flow rate of the air affects by nearly 3% the variation rate of the average cell temperature among different cells when the boundary condition is adiabatic. Nevertheless, the effect of a non-uniform inlet flow of the air can be ignored when the boundary condition is a constant temperature. Although the effect of the non-uniform inlet molar flow rate does not affect the total power of the SOFC stack, the variation rate of the average cell temperature and cell voltage is close to 3% and 15%, respectively. This non-uniform effect on the electrical performance of each stack is apparently larger than in the transverse direction, which was examined in our previous research [20].

Acknowledgement

This study was supported by the National Science Council, the Republic of China, through grant number NSC 96-2221-E-234-002.

References

[1] J.R. Ferguson, J.M. Fiard, R. Herbin, J. Power Sources 58 (1996) 109–122.
[2] H. Yakabe, M. Hishinuma, M. Uratani, Y. Matsuzaki, I. Yasuda, J. Power Sources 86 (2000) 423–431.
[3] H. Yakabe, T. Ogiwara, M. Hishinuma, I. Yasuda, J. Power Sources 102 (2001) 144–154.
[4] J. Yuan, M. Rokni, B. Sunden, Numer. Heat Transf. A: Appl. 39 (2001) 801–822.
[5] J. Yuan, M. Rokni, B. Sunden, Numer. Heat Transf. A: Appl. 43 (2003) 341–366.
[6] J.J. Huang, C.K. Chen, D.Y. Lai, J. Power Sources 140 (2005) 235–242.
[7] V.M. Janardhanan, V. Heuveline, O. Deutschmann, J. Power Sources 172 (2007) 296–307.
[8] T. Araki, T. Ohba, S. Takezawa, K. Onda, Y. Sakaki, J. Power Sources 158 (2006) 52–59.
[9] S. Bedogni, S. Campanari, P. Iora, L. Montelatici, P. Silva, J. Power Sources 171 (2007) 617–625.
[10] E. Achenbach, J. Power Sources 49 (1994) 333–348.
[11] K.P. Recknagle, R.E. Williford, L.A. Chick, D.R. Rector, M.A. Khaleel, J. Power Sources 113 (2003) 109–114.
[12] S.B. Beale, Y. Lin, S.V. Zhubrin, W. Dong, J. Power Sources 118 (2003) 79–85.
[13] M. Iwata, T. Hikosaka, M. Morita, T. Iwanari, K. Ito, K. Onda, Y. Esaki, Y. Sakaki, S. Nagata, Solid State Ionics 132 (2000) 297–308.
[14] Y. Wang, F. Yoshiba, T. Watanabe, S. Weng, J. Power Sources 170 (2007) 101–110.
[15] P. Costamagna, E. Arato, E. Achenbach, U. Reus, J. Power Sources 52 (1994) 243–249.
[16] R.J. Boersma, N.M. Sammes, J. Power Sources 66 (1997) 41–45.
[17] T. Okada, S. Matsumoto, M. Matsumura, M. Miyazaki, M. Umeda, J. Power Sources 162 (2006) 1029–1035.
[18] H. Hirata, M. Hori, J. Power Sources 63 (1996) 115–120.
[19] S.F. Liu, H.S. Chu, P. Yuan, J. Power Sources 161 (2006) 1030–1040.
[20] P. Yuan, S.F. Liu, Numer. Heat Transf. A: Appl. 51 (2007) 941–957.
[21] J.H. Koh, H.K. Seo, Y.S. Yoo, H.C. Lim, Chem. Eng. J. 87 (2002) 367–379.
[22] L.J.M.J. Blomen, M.N. Mugerwa, Fuel Cell Systems, Plenum Press, New York, 1993, pp. 73–75.
[23] S.H. Chan, K.A. Khor, Z.T. Xia, J. Power Sources 93 (2001) 130–140.
[24] J. Larminie, A. Dicks, Fuel Cell Systems Explained, 1st ed., Wiley, West Sussex, 2000, p. 53.
[25] R. Maric, S. Ohara, T. Fukui, H. Yoshida, M. Nishimura, T. Inagaki, K. Miura, J. Electrochem. Soc. 146 (1999) 2006–2010.
[26] A.L. Hines, R.N. Maddox, Mass Transfer Fundamentals and Applications, Prentice-Hall, New Jersey, 1985, pp. 17–59.